

Dynamics of EEG Entropy: beyond signal plus noise

M. Ignaccolo¹, M. Latka², W. Jernajczyk³, P. Grigolini⁴ and B.J. West^{1,5}

1) Physics Department, Duke University, Durham, NC

2) Institute of Biomedical Engineering, Wrocław University of Technology, Wrocław, Poland

3) Department of Clinical Neurophysiology, Institute of Psychiatry and Neurology, Warsaw, Poland

4) Center for Nonlinear Science, University of North Texas, Denton, TX

5) Mathematics and Information Science Directorate, Army Research Office

(Dated: September 3, 2021)

EEG time series are analyzed using the diffusion entropy method. The resulting EEG entropy manifests short-time scaling, asymptotic saturation and an attenuated alpha-rhythm modulation. These properties are faithfully modeled by a phenomenological Langevin equation interpreted within a neural network context. Detrended fluctuation analysis of the EEG data is compared with diffusion entropy analysis and is found to suppress certain important properties of the EEG time series.

PACS numbers:

I. INTRODUCTION

The mammalian brain generates a small but measurable electrical signal; first measured in small animals by Caton in 1875 and in people by Berger in 1925. The trace left on a strip chart by this amplified signal was called an electroencephalograph and the term electroencephalogram (EEG) has subsequently been used to identify the electrical signal. The power associated with the EEG signal is distributed over the frequency interval 0.5 to 100 Hz, with most of it concentrated in the interval 1 to 30 Hz. A typical EEG signal looks like a random time series with contributions from every part of the spectrum appearing with random phases. In the nearly one hundred years since the electroencephalogram (EEG) was introduced into neuroscience there have been a variety of methods used in attempts to establish a taxonomy of EEG patterns in order to delineate the correspondence between brain wave patterns and brain activity. The mathematician Norbert Wiener proposed *generalized harmonic analysis* [1] as the mathematical tool necessary to penetrate the mysterious relations between the EEG time series and the functioning of the brain. Subsequently, spectral methods have figured prominently in characterizing the properties of EEG time series. More recently nonlinear processing techniques, with their implicit dependence on nonlinear dynamics, chaos and fractals have lead the parade of methodologies hoping to accomplish this task, see, for example, West [2] for a brief review. The progress in relating EEG patterns to brain function has been slow and the understanding and interpretation of EEG signals remain elusive. However certain properties of EEG signals have revealed themselves over time.

Over the past half century the single channel EEG time series has been interpreted as consisting of relatively slow regular variations called *signal*, which is the integrated contribution of the neurons in the vicinity of the channel lead along with the 'coherent' influence of distant neurons, and the relatively rapid erratic fluctuations called *noise*, which is the 'incoherent' contribution of the distal neurons in the brain. However, the erratic behavior of the EEG time series is so robust that it persists through all but the most drastic situations including near-lethal levels of anesthesia, several minutes of asphyxia and the complete surgical isolation of a slab of cortex [3]. This separation implies that the signal contains information about the particular neurons associated with the EEG channels in the brain, whereas the erratic fluctuations are a property of a channel's environment and does not contain any useful information. Recent studies have refined this engineering model of signal plus noise and extracted information from the random fluctuations by concentrating on what is believed to be the scaling behavior of EEG time series.

A number of research groups [4, 5, 6, 7, 8] have recently determined that EEG time series $X(t)$ have scaling properties, with a second moment that increases as a non-trivial power-law, that is, $\langle X(t)^2 \rangle \propto t^{2H}$. Here the brackets denote a suitably defined averaging over the data. In random walk models of classical diffusion the scaling exponent would be given by $H = 0.5$, whereas sub-diffusion processes would have $H < 0.5$ and super-diffusion processes would have $H > 0.5$. The index H was introduced by Mandelbrot into the study of the long-time memory of the statistical fluctuations of time series in recognition of Hurst who first observed such an effect in the yearly river flow of the Nile. The spectrum $S(f)$ associated with such time series fall in the category of $1/f$ noise, that is, the Fourier transform of the autocorrelation function is given by $S(f) \propto 1/f^\beta$ with frequency f and power-law index related to the Hurst exponent by $\beta = 2H - 1$, consequently the if the index falls within the interval $0 \leq \beta \leq 1$ the underlying process is super-diffusive. However the spectral index can be greater than one for general complex phenomena such as EEG time series. In general however the spectral approach is not reliable because the EEG time series are non-stationary and consequently their direct Fourier transforms are ill-defined.

The 'signal' parts of the EEG time series are called waves or rhythms. The nature and scope of these waves have been widely investigated, see Başar [9] for a review. The alpha rhythm (7-12 Hz) has been shown to be typical of awake individuals when the brain is under no stimulation. Başar et al.[10] have developed an integrative theory of alpha oscillations in brain functioning. They hypothesize that there is not one, but several alpha-wave generators distributed within the brain and note that the alpha rhythm may act as a nonlinear clock in the manner suggested by Wiener [1] to serve as a gating function to facilitate the association mechanisms within the brain.

The method of choice [4, 5, 6, 7, 8], used to address the issue of non-stationarity in EEG signals, is detrended fluctuation analysis (DFA) which provides a measure of the standard deviation of the detrended fluctuations [11]. This method of processing EEG time series to determine scaling behavior consistently finds fractal properties, such as those observed in earlier studies. DFA has been used to quantify the scaling property of EEG dynamics by direct application to EEG signals [5, 8] and to EEG increments [4]. Buiatti et al. [12] use DFA to show that specific task demands can modify the temporal scale-free dynamics of the ongoing brain activity as measured by the scaling index. Watters and Martin [6] recognized the two scaling regimes observed in the processing of EEG time series by a number of investigators and proposed zero-crossings as an alternative method of analysis in order to focus on the long-time correlations in the EEG signal. They dichotomize the EEG series according to the zero crossing time series and apply DFA to the dichotomized EEG. Stead et al. [7] apply DFA to the energy, that is to the square modulus, of an EEG signal. Finally, the authors of [13] analyzed the histograms for the DFA detrended EEG time series to estimate the associated probability density function (*pdf*) and its scaling properties.

The observed scaling in EEG time series is not as straightforward as that observed in other less complex phenomena. Hwa [4], for example, finds that the standard deviation of the EEG fluctuations exhibit two distinct scaling regions, whose variability was analyzed through a moment technique that could discriminate between normals and those that had undergone a stroke with up to 90% accuracy. Robinson [14], on the other hand, in his analysis of EEG time series demonstrated the existence of scaling up to a point in time after which saturation in the standard deviation occurs. He attributed this saturation effect to "dendritic filtering" and the DFA averaging the influence of the shape of the spectrum on the time series. Finally, DFA has been used to study eventual correlation of the alpha rhythm [15, 16]

Various measures other than the standard deviation, spectrum and the distribution of zero crossings have been introduced into the study of EEG time series, each one stressing a different physiologic property thought to be important in representing the brain's dynamics. One recent measure introduced to quantify the level of coherence in EEG signals is entropy. However, the entropy of Boltzmann and the information entropy of Shannon would not be immediately evident in many of these studies. For example, Inouye et al. [17] employed spectral entropy, as defined by the Fourier power spectrum, but the fact that EEG time series are not stationary, in the sense that the autocorrelation function is not simply a function of the two-time difference, obviates the use of Fourier transforms. Schlögl et al. [18] measured the information entropy of 16 bit EEG polysomnographic records and found it to be in the range of 8-11 bits. Patel et al. [19], using a combination of fMRI and entropy maximization, where the probability density in the entropy definition is replaced with a scaled dipole strength, demonstrated that the generators of alpha rhythm are mainly concentrated over the posterior regions of the cortex, consistent with the theoretical speculations of others [10]. Subsequently, wavelet entropy, in which the probability density is replaced with the relative wavelet energy, was used by Rosso et al. [20, 21] to study the order/disorder dynamics in short duration EEG signals including evoked response potentials.

In Section II we introduce stochastic differential equations as a way to model complex phenomena. The *pdf* determined by the stochastic equations are used to construct the diffusion entropy (DE), which is shown to be a viable measure of the dynamic mechanisms introduced into such stochastic models. DE analysis is also used to process EEG time series data and consequently suggests a form for the stochastic dynamical equations with which to model the observed EEG properties. Section III introduces the signal plus noise paradigm of signal processing, which is arguably the basis for DFA, recently the favored technique in the neuroscience literature for the analysis of EEG time series. The EEG models developed in Section II are shown to lead to much different conclusions regarding the scaling of EEG data depending on whether the DE or DFA methods are used for their analysis. The coherence of alpha wave is discussed in Section IV to explain why the alpha-wave modulation of the EEG entropy is attenuated over time. Finally, we draw some conclusions in Section V.

II. EEG MODELS

Most recently the authors [22] have used the DE method [23] to characterize the EEG time series dynamic properties. This technique had been successfully used previously to discriminate between the contributions of low-frequency waves (signal) and high-frequency fluctuations (noise) in a number of other phenomena, for example, to determine the seasonal influence on the daily number of teen births in Texas [24]; the effect of solar cycles on the statistics of solar flares [25]; the influence of solar dynamics on the average global temperature anomalous fluctuations [26]. Herein we

use the DE method to provide insight into the low/high frequency dynamics of EEG time series and compare those results with processing of the same data using DFA.

A. Ornstein-Uhlenbeck Langevin equation

In the physics literature there are two strategies for treating stochastic phenomena, those involving stochastic differential equations for the dynamic variables and those involving the partial differential equations of evolution for the probability density in phase space. The former are called collectively Langevin equations and the latter Fokker-Planck equations. Here we use a Langevin equation to model the EEG time series because it enables us to isolate the various physiologic mechanism that might contribute to the signal. For review consider the Ornstein-Uhlenbeck (OU) Langevin equation for a linearly dissipative stochastic process

$$\frac{dX(t)}{dt} = -\lambda X(t) + \xi(t) \quad (1)$$

where the random force $\xi(t)$ is delta correlated in time with strength D and has Gaussian statistics

$$\langle \xi(t) \xi(t + \tau) \rangle = 2D\delta(\tau), \quad (2)$$

where the symbol $\langle \dots \rangle$ indicates the ensemble average. Here there are two physical mechanisms; the heat bath modeling the environment giving rise to the random force and the dissipation modeling the average energy extracted from the dynamic system by the environment, see for example, Lindenberg and West [27]. In a physical system the fluctuations and dissipation are interdependent through the Einstein relation

$$\frac{D}{\lambda} = kT \quad (3)$$

in order for the system to be thermodynamically closed. Equation (3) is also known as the fluctuation-dissipation relation, which defines the equilibrium temperature of the heat bath in terms of the ratio of the strength of the fluctuations to the dissipation rate.

The variance of the dynamic process

$$\sigma^2(t) \equiv \langle X^2(t) \rangle - \langle X(t) \rangle^2 \quad (4)$$

is given here, using the solution to the OU Langevin equation,

$$\begin{aligned} \sigma^2(t) &= \int_0^t dt_1 e^{-\lambda(t-t_1)} \int_0^t dt_2 e^{-\lambda(t-t_2)} \langle \xi(t_1) \xi(t_2) \rangle \\ &= \frac{D}{\lambda} [1 - e^{-2\lambda t}]. \end{aligned} \quad (5)$$

Consequently, for $t \ll 1/\lambda$ the variance increases linearly with time

$$\lim_{t \rightarrow 0} \sigma^2(t) \approx 2Dt \quad (6)$$

so that the scaling index is $H=0.5$. For $t \gg 1/\lambda$ the variance becomes time independent

$$\lim_{t \rightarrow \infty} \sigma^2(t) = \frac{D}{\lambda}, \quad (7)$$

with a saturation induced by the dissipation. In the engineering literature the dissipation is called a filter and its influence on the time series is a negative feedback reducing the difference between the observed and desired signal. It

is this uncontrolled difference, the noise, that is observed in the asymptotic saturation level given by the ratio of the strength of the fluctuations and the dissipation rate.

The solution to the Langevin equation defines a trajectory. An ensemble of such trajectories, generated by the random force, is used to construct the histogram of the number of trajectories falling in a specified interval to estimate the *pdf* $p(x, t)$. The *pdf* can then be used to calculate the information entropy, a quantity introduced in discrete form for coding information by Shannon [28] and in continuous form for studying the problem of noise and messages in electrical filters by Wiener [29]. We use the latter form here,

$$S(t) = - \int p(x, t) \log_2 p(x, t) dx. \quad (8)$$

Given the Gaussian statistics of the random force in the OU Langevin equation we know that the statistics of the dynamical variable are also Gaussian. Substituting a Gaussian distribution with a variance $\sigma^2(t)$ into (8) we obtain

$$S(t) = \log_2 \left(\sqrt{2\pi e} \sigma(t) \right). \quad (9)$$

Consequently, for $t \ll 1/\lambda$ using the approximate variance of Eq. (6) the entropy increases as

$$\lim_{t \rightarrow 0} S(t) = \frac{1}{2} \log_2 (4\pi D e) + \frac{1}{2} \log_2 t \quad (10)$$

and a linear-log plot yields a straight line of slope $H=0.5$. At the other extreme $t \gg 1/\lambda$ using the approximate variance (7) the entropy reaches the saturation level

$$\lim_{t \rightarrow \infty} S(t) = \frac{1}{2} \log_2 \left(\frac{2\pi D e}{\lambda} \right). \quad (11)$$

This use of information entropy is suggestive in that it shares certain properties with the EEG analysis discussed in the Introduction that being scaling behavior at early times followed by asymptotic saturation. We exploit these two mathematical properties of the OU Langevin equation in the Section IIC to develop a dynamical model of EEG time series.

B. EEG data analysis

Each single channel recording of the EEG time series consists of a sequence of $N + 1$ data points, and the difference between successive data points is denoted by ξ_j for $j = 1, 2, \dots, N$. For the DE analysis of the EEG data a set of diffusive variables $X_k(t)$ is constructed from the differenced data points in the following way

$$X_k(t) = \sum_{j=k}^{k+t} \xi_j, \quad k = 1, 2, \dots, N - t + 1 \quad (12)$$

to obtain $M = N - t + 1$ replicas of a diffusive trajectory using overlapping windows of length t . An ensemble of such trajectories, generated by the EEG time series, is used to construct the histogram from the number of trajectories falling in a specified interval to estimate the *pdf*. Note that this is analogous to what we did in the previous section, the procedural difference is that here we use data to define the trajectory and not the solution to a Langevin equation. Another difference is that we do not know the form of the *pdf* that results from the histogram. However we can anticipate a class of *pdf*'s based on previous investigations. For example Schlögl *et al.* [18] observed a deviation from Gaussian behavior with a time-dependent variance, but with nearly symmetric empirical distribution functions. We assume here, but latter establish a theoretical model, a simple analytical form for the *pdf* of the diffusion process that satisfies the scaling relation:

$$p(x, t) = \frac{1}{\sigma(t)} F \left(\frac{x}{\sigma(t)} \right). \quad (13)$$

Note that a Gaussian diffusion process satisfies (13) with a time-dependent standard deviation $\sigma(t)$. More generally an alpha-stable Lévy process also scales in this way, in which case $\sigma(t)$ is more general than the standard deviation of the underlying process. The scaling condition so often anticipated in EEG time series implies that

$$\sigma(t) = kt^\delta, \quad (14)$$

where k is a constant. Substituting Eqs. (13) and (14) into Eq. (8) yields

$$S(t) = - \int F(y) \log_2 F(y) dy + \log_2 k + \delta \log_2 t = C + \delta \log_2 t. \quad (15)$$

This diffusion entropy graphed versus time on log-linear graph paper would increase linearly with slope δ with an initial level determined by the constant C . Consequently, the way in which the entropy for a time series scales is indicative of the scaling behavior of the underlying time series and consequently of the *pdf*. Note that in a simple diffusive process this scaling index is equal to the one obtained from calculating the second moments, that is, $\delta=H$. However, in general, even when the data do scale the two power-law indices are not necessarily equal and $\delta \neq H$.

We now consider EEG signals of twenty awake individuals in the absence of external stimulations (quiet, closed eyes). EEG signals were recorded using the 10-20 international recording scheme. For eight individuals only the channels O1,O2,C3 and C4 were recorded, for the remaining twelve all the channels are available. To have a consistent database, we restrict our analysis to the channels O1,O2,C3 and C4, which are the channels traditionally used in sleep studies. The sampling frequency of all EEG records is 250Hz, and durations of EEG records vary from 55s to 400s with an average duration of 128.1s.

Fig. 1 shows the DE of the EEG increments for the somnographic channels O1,O2,C3 and C4 of a single individual. We see how for each channel the EEG diffusion entropy: 1) reaches a saturation level, 2) has an ‘‘alpha’’ (~ 7.6 HZ in the case of this individual) modulation which is attenuated with time, and 3) has a small amplitude residual asymptotic modulation. The early-time modulation, with variable frequency in the alpha range and variable amplitude, is observed in the somnographic channels for all subjects. The saturation effect is present in all channels for all subjects and it should be pointed out that this saturation is neither a consequence of the finite length of the time series, nor of the finite amplitude of the EEG signal. In fact when we randomly rearranged the data points, thereby destroying any long time correlation in the time series, the EEG entropy no longer saturates. Consequently, this saturation effect is due to correlated brain dynamics and is not an artifact of the data processing. The inset in Fig. 1 depicts the *pdfs* $p_{\text{sat}}(x)$, after the entropy saturation is attained. These distributions have approximately exponential tails. Fig. 2 depicts the diffusion entropy for the nineteen channels of a representative individual. In this figure the somnographic channels have strong alpha rhythms, but the other channels do not. However it is evident that regardless of the alpha wave content of the EEG time series each and every channel saturates.

C. EEG Langevin equation

The simplest dynamic model, which includes all the properties identified in Fig. 1, these being, fluctuations, modulation and dissipation, has the form of a Langevin equation. We assume a dissipative linear dynamic process dynamic process $X(t)$, i.e., an OU process, with a periodic driver having a random amplitude and frequency and an additive random force $\eta(t)$ which is a delta correlated Gaussian process of strength D :

$$\frac{dX(t)}{dt} = -\lambda X(t) + \eta(t) + \sum_{j=0} A_j \chi [I_{j,s}] \sin [2\pi f_j t] \quad (16)$$

The coefficient λ is positive definite and defines a negative feedback, $\chi [I_{j,s}] = 1$ when the argument of $\chi []$ is the time interval $I_{j,s} = [jt_s, (j+1)t_s]$ and is zero otherwise, and t_s is the ‘stability’ time after which a new constant frequency f_j and a new constant amplitude A_j are selected.

The values of the frequencies f_j and amplitudes A_j are empirical and determined in the following way. First, we evaluate the spectral density in the time-frequency domain of time series of EEG increments with a time resolution t_s and a frequency resolution Δf by means of a Windowed Fourier Transform. The theoretical spectral density is estimated from the spectrogram, which is the spectrum of a time series for a given time resolution, but which changes as a function of time. Therefore there is no one spectrum to characterize the process as we sweep through the non-stationary EEG time series, see the discussion on spectrograms in Ref. [30]. The spectral density, or spectrogram, is a three-dimensional plot of the spectrum of the EEG increments ξ_j as it changes over time. Then, for each time interval of duration t_s we consider the range of frequencies of the alpha waves, 7-12 Hz, and find which frequency has the maximum amplitude in the spectrogram. This procedure defines the frequency and the amplitude of the time interval considered.

Panel (a) of Fig. 3 shows the spectrogram relative to the increments ξ_j of the channel O1 for the same subject as in Fig. 1. Panels (b) and (c) of Fig. 3 show respectively the sequence of amplitudes A_j (normalized to a maximum amplitude of 1) and of frequencies f_j calculated using the procedure described above. Without an *a priori* knowledge of the typical duration of an alpha wave packet, we set the stability time t_s of Eq. (16) equal to 0.5s. A time resolution

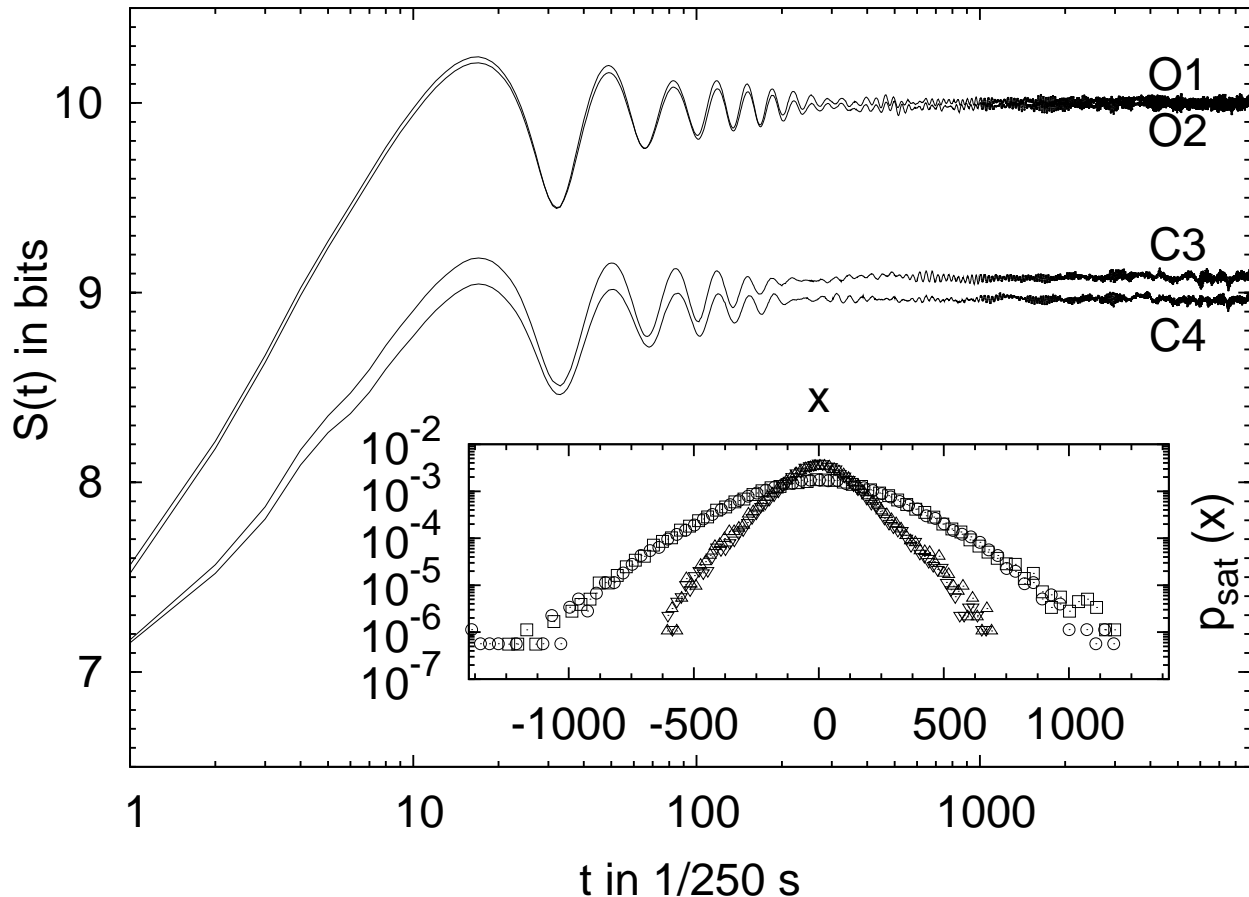


FIG. 1: The diffusion entropy $S(t)$ calculated using the increments of the channels O1, O2, C3 and C4 for one of the 20 subjects considered in this study. The inset depicts the asymptotic pdfs $p_{\text{sat}}(x)=p(x, t = 2000)$ for each channel: squares (O1), circles (O2), upward triangles (C3), and downward triangles (C4).

of 0.5s and a frequency resolution of approximately 0.5Hz in the spectrogram represent a reasonable time-frequency localization for our purposes.

When the modulation is present Eq.(16) is numerically integrated, and the increments of the dynamic variable X are processed using the DE algorithm. In Fig. 4, we compare the EEG entropy obtained using the integrated solutions of Eq. (16) with that of the channels O1 and C3, already shown in Fig. 1. It is evident that the entropy constructed from the solution to Eq.(16) captures the qualitative and many of the quantitative features of the DE of the EEG increments. Moreover, the asymptotic *pdfs* recorded in the inset also agree with the empirical *pdfs* depicted in Fig. 1. In Table 1 we average the phenomenological parameters λ and D for the somnographic channels for the twenty subjects in this study. Note that both the strength of the fluctuations and the dissipation rates change between the O1, O2

TABLE I: The average values (avg.) and the standard deviations (s.d.) of the parameters λ and D of Eq. (16) for all 20 subjects in this study.

EEG channel	λ (avg. \pm s.d.)	D (avg. \pm s.d.)
O1	0.0461 \pm 0.0187	16.37 \pm 6.88
O2	0.0497 \pm 0.0182	16.35 \pm 6.72
C3	0.0362 \pm 0.0186	10.19 \pm 3.90
C4	0.0393 \pm 0.0200	10.60 \pm 3.72

values and the C3, C4 values. This suggests that the channel environment changes in a statistically significant way

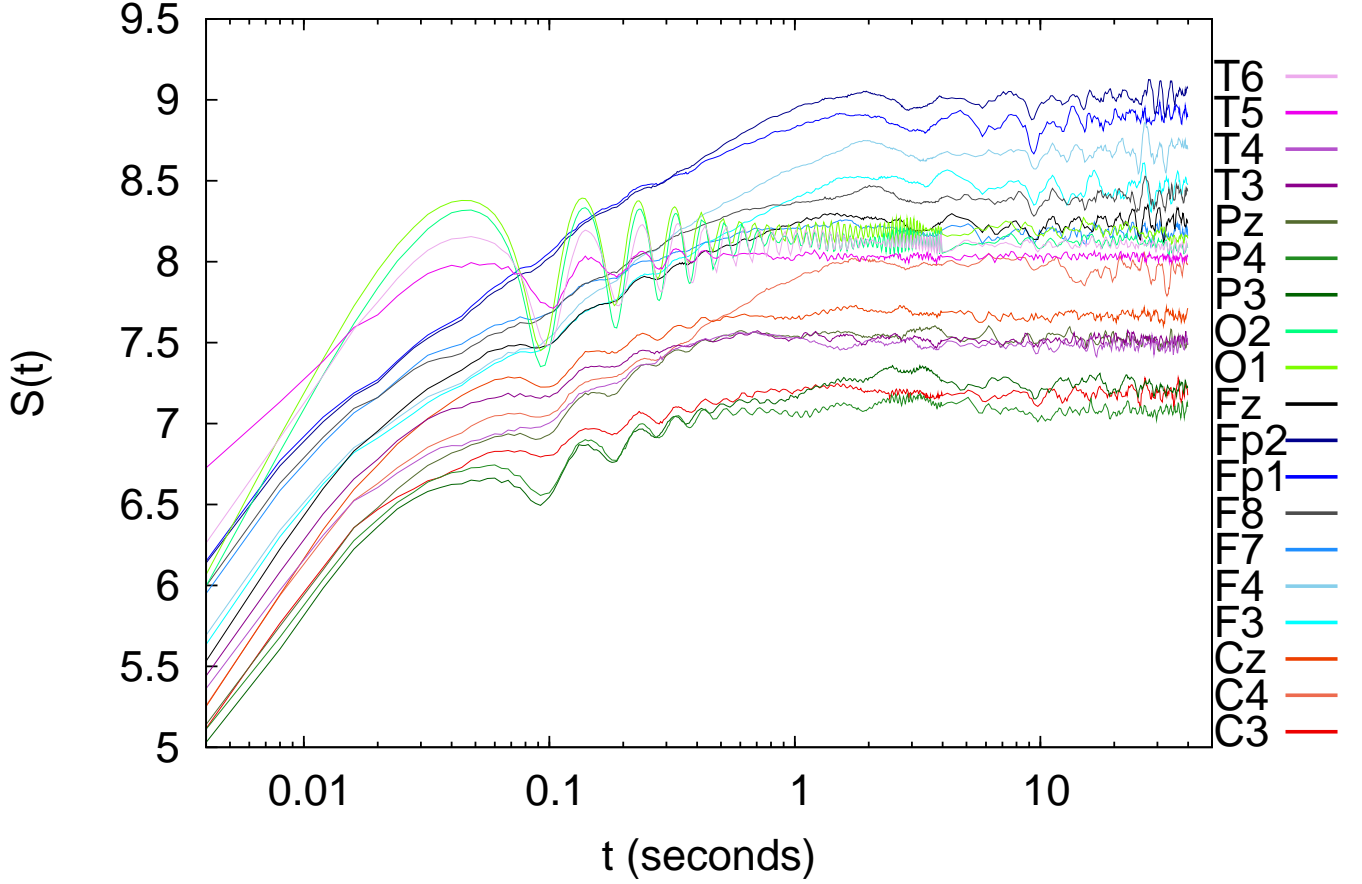


FIG. 2: The diffusion entropy $S(t)$ of the EEG increments of all the 19 channels for one of the 20 subjects considered in this study.

from one region of the brain to another, with the O1, O2 channels being noisier and more dissipative.

III. DIFFUSION ENTROPY ANALYSIS VERSUS DFA

In Sec. II, we showed how the properties of the EEG records can be modeled using an OU Langevin equation: The solution to Eq. (16) if the EEG record has an alpha rhythm (the generalization to a different rhythm or a sum of two or more rhythms is straightforward), and the solution to Eq. (1) if no rhythm is present. As stated in the Introduction, a main tenet of the traditional EEG analysis is the decomposition of an EEG record X_j into the sum of two orthogonal components:

$$X_j = S_j + N_j \text{ AND } \text{Cov}(S, N) = 0 \quad (17)$$

where S_j is the time varying mean or *signal* (rhythms), N_j is the *noise* or random component and $\text{Cov}(S, N)$ is the covariance of the two. DFA was introduced [11] as a tool to measure the scaling of the variance of the noise component of a time series N_j without *a priori* knowledge of the signal component of the time series S_j . For this reason, as well as the fact that it apparently works for time series that scale, DFA has been widely used in the analysis of EEG time series.

However, the signal plus noise decomposition of Eq. (17) is not applicable to the OU processes or the driven OU processes of Eqs. (1) and (16), respectively. The solution to Eq. (1) is

$$X(t) = e^{-\lambda t} \int_0^t \eta(t') e^{\lambda t'} dt' \quad (18)$$

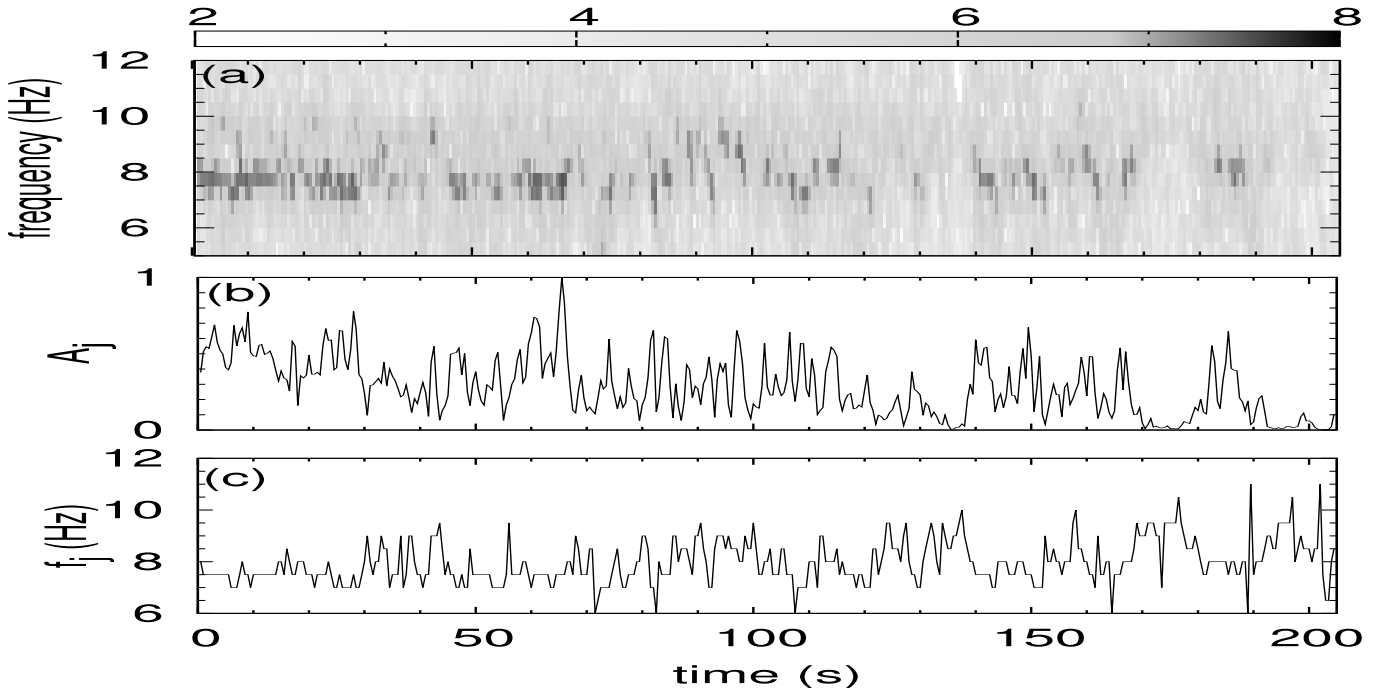


FIG. 3: (a) Spectrogram of the increments of channel O1. We plot the base-10 logarithm of the spectral density. The time resolution is $t_s=0.5$ s, the frequency resolution is $\Delta f=0.5$ Hz. (b) Sequence of the maxima of the spectrogram amplitude (normalized so that the maximum amplitude is 1). This sequence of coefficients A_j is used in Eq. (16). (c) Sequence of the frequencies corresponding to the amplitude maxima of the spectrogram. This sequence of coefficient f_j is used in Eq. (16).

where we assumed, without loss of generality, that $X(0)=0$. In this case we have no *signal* component. Moreover, Eq. (18) states that the present value of $X(t)$ depends on all the previous history. In particular, the autocorrelation function $\Phi_\xi(t)$ of the increments $\xi(t)=d/dtX(t)$ is negative with an exponential decay:

$$\Phi_\xi(t) = \frac{d}{dt^2}\sigma^2(t) = \delta(t) - 4D\lambda \exp(-2\lambda t), \quad (19)$$

where $\delta(t)$ is the Dirac delta function. A consequence of Eq. (19) is that the power spectrum of the increment time series $\xi(t)$ does not satisfy the relation $S(f) \propto 1/f^\beta$. Applying the Wiener–Khinchine theorem to Eq. (19), we obtain

$$S(f) = \frac{1}{2} \left[1 - \frac{4\lambda^2}{4\lambda^2 + 4\pi^2 f^2} \right] \quad (20)$$

and consequently the spectrum is zero at low frequencies and increases quadratically to a constant value at high frequencies. But let us consider the more general case, using the solution of Eq. (16), assuming $X(0)=0$,

$$X(t) = e^{-\lambda t} \int_0^t \left\{ \eta(t') + \sum_{j=0} A_j \chi [I_{j,s}] \sin(2\pi f_j t') \right\} e^{\lambda t'} dt'. \quad (21)$$

If we identify the alpha-wave component, the second term under the integral, as the *signal* then it is *not* possible to separate $X(t)$ according to Eq. (17). In particular the covariance $\text{Cov}(S, N)$ does not vanish because the present value of $X(t)$ depends on its previous values. As for the covariance function of the increments in this case, the behavior of Eq. (19) is periodically modulated, while the power spectrum shows a peak in the alpha range as shown in Fig. 5.

For these reasons, in this section, we compare the results of DFA and DE when applied to EEG records, and to records (via numerical integration) of the OU processes of Eqs. (1) and (16). We set the length of these records to be 50,000 to match the typical length of the EEG records examined herein: 50,000 data points is equivalent to 200 seconds of data with a 250Hz sampling frequency.

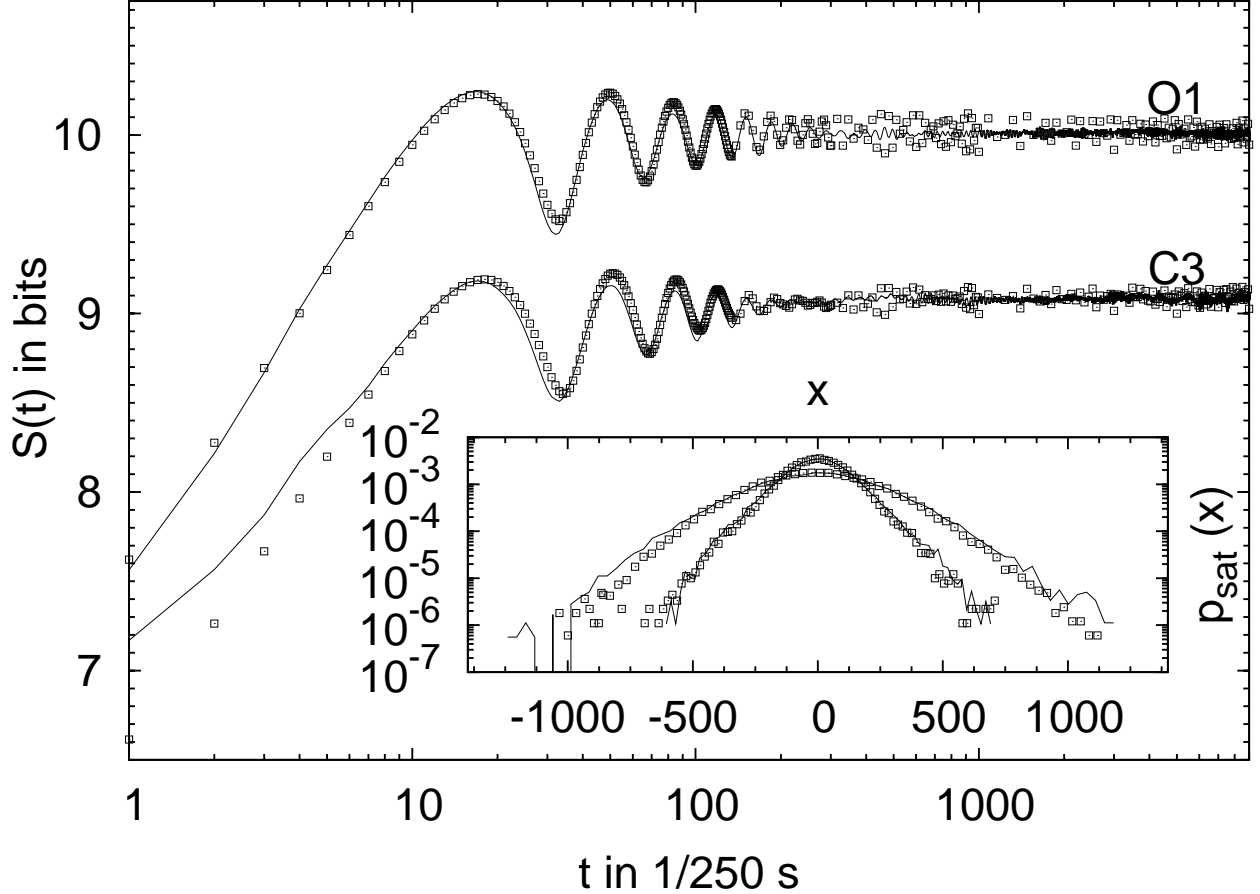


FIG. 4: Comparison between the diffusion entropy of the increments, solid lines, of channel O1 and C3, and diffusion entropy of the increments, points, of the variable X of Eq. (16). The parameters used in Eq. (16) are $\lambda=0.055$ $D=40$ for O1 and $\lambda=0.055$ $D=20$ for C3. Inset show the comparison between the asymptotic pdfs $p_{\text{sat}}(X)=p(X, t=2000)$: channels O1 and C3, solid lines, variable X of Eq. (16), squares.

First, we briefly describe the DFA algorithm. Given a time series X_k , the zero-averaged time series is aggregated

$$Y_j = \sum_{k=1}^{k=j} [X_k - X_{avg}] \quad (22)$$

where X_{avg} is the average of the time series X_k . The integrated signal is divided into windows of size t . Here we use overlapping windows adopting the same procedure as the DE algorithm (Sec. II B), while the original algorithm uses non-overlapping windows [11]. For each window, a least-squares fit is computed with a polynomial of order $n \geq 1$. This fitting procedure eliminates the local trend: the *signal* in that particular window. Finally the local trend is subtracted from the integrated time series and the standard deviation of the residuals \tilde{Y}_j calculated:

$$F(t) = \sqrt{\frac{1}{t} \sum_{j=1}^t \tilde{Y}_j^2}. \quad (23)$$

These steps are repeated for increasing values of the window size t . The scaling condition for the standard deviation implies

$$F(t) \propto t^\alpha \Leftrightarrow \log_2 F(t) \propto \alpha \log_2 t \quad (24)$$

where the scaling parameter is in the interval $0 \leq \alpha \leq 1$.

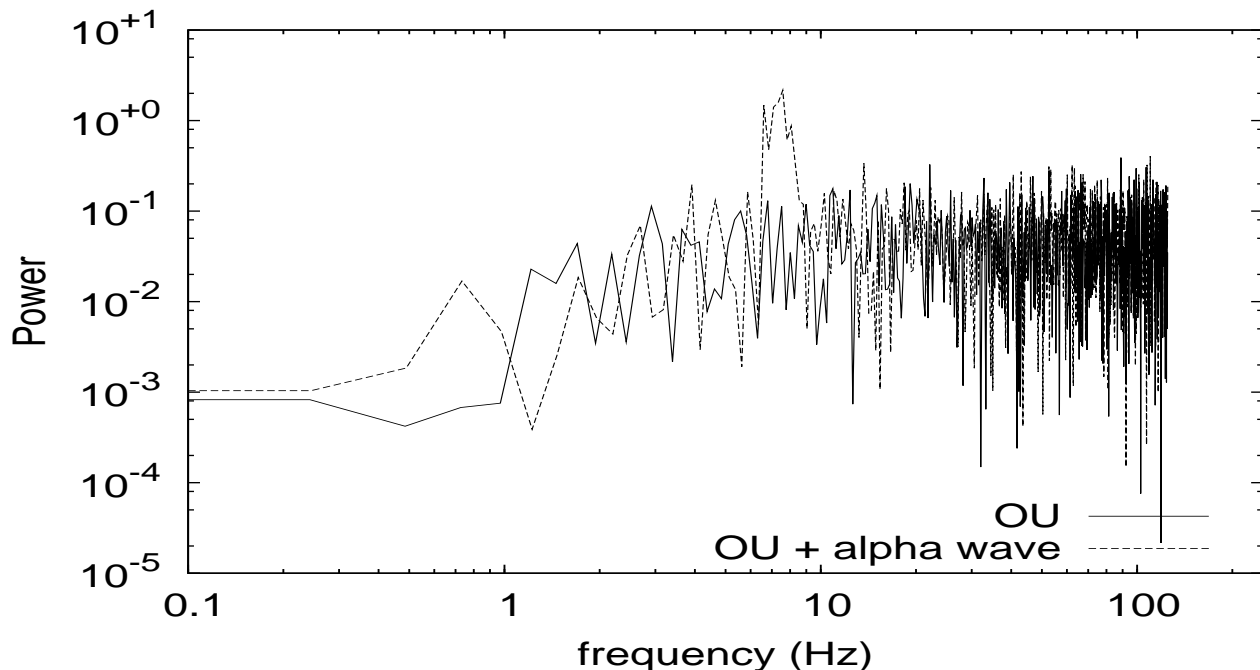


FIG. 5: The solid line depicts the power spectrum of the increments of the variable $X(t)$ of Eq. (18) ($\lambda=0.055$ and $D=800$), the dashed line depicts the power spectrum of the increments of the variable $X(t)$ of Eq. (21) ($\lambda=0.055$, $D=800$ and alpha wave coefficients of the channel O1 of Fig .1).

In Fig. 6, we plot the results of DE and DFA when applied to the time series of the increments of the variable $X(t)$ of Eq. (1) with $\lambda=0.055$ and $D=800$. The DE (triangles) agrees [31] with the theoretical prediction of Eq. (9) (solid line). Moreover, the DE results show that the approximation given by Eq. (10) for the case $\lambda=0.055$ is valid up $\sim 0.02-0.03s$ (note that the factor $1/\lambda$ must be divided by the value of sampling frequency which is 250Hz). DFA results (circles for a linear detrending and squares for a quadratic detrending) show hints of a saturation regime more than two decades later than it actually occurs: $\sim 10s$ instead of $\sim 0.1s$. As for the expected initial regime $F(t) \propto \sqrt{t}$ (Eq. (6)), one can linearly fit the DFA curves in different ranges for times $t \lesssim 0.4s$ (before the strong “bending” occurs in the DFA). The results depend on the particular fitting range used: e.g. in the range $0.04s \leq t \leq 0.4s$ the resulting slope (for the DFA curve obtained with a linear detrending) is $\simeq 0.44$.

Fig. 7 shows the results of the DE method and DFA for the increments of a EEG record (channel O1) and the increments of its best approximation via the model of Eq. (16) (Section II C). We notice how the results, for both DE and DFA, relative to the OU process of Eq. (16) (triangles for DE and circles and squares for DFA) reproduce those relative to the EEG record (solid line). We notice how the presence of the alpha rhythm results in an initial ($t < 0.04s$) slope of the diffusion entropy $S(t)$ which is larger than 0.5 as expected with no alpha rhythm Eq. (10): for times smaller than the typical period of the alpha rhythm, the alpha rhythm is “equivalent” to a trend which produce an additional entropy increase (for detailed discussion of this effect see [24], for example. As for the results of DFA, we see how the modulation due to the alpha-wave packets has been eliminated and instead two “slopes” are observed for $t \lesssim 0.2s$. As in Fig. (6) DFA approaches a saturation regime two decades later than what expected from the model of Eq. (16) and correctly detected by the DE. For the DFA curve obtained with a quadratic detrending, we have: slope 0.65 for $0.01s < t < 0.06s$, slope 1.2 for $0.08s < t < 0.2s$, and slope 0.1 for $0.3s < t < 1.6s$. These results indicate that the DFA is not able to accurately “detrend” the periodic component (alpha wave) and the observed linear regimes are not actual scaling regimes. In Figs. 6 and 7, we have applied the DE and the DFA to the increments of the variable $X(t)$ (Eq. (1) for Fig. 6 and Eq. (16) for Fig. 7) or to the EEG increments ξ_j . Some investigators [4] use DFA to analyze the resting (closed eye) EEG of normal subjects and of subjects with acute ischemic stroke. They report the presence in virtually all channel and for all subjects of a “double” scaling regime in the time ranges corresponding to the second and third linear regimes of Fig. 6. The reported [4] ranges of values for the scaling parameters are compatible with the one calculated for Fig. 6. However the analysis presented in this manuscript suggest that these linear regimes observed in the DFA are not genuine scaling regimes but are the result of the EEG dynamics not satisfying the signal plus noise decomposition of Eq. (17) thereby compromising the capability of the DFA to detrend the alpha-wave component.

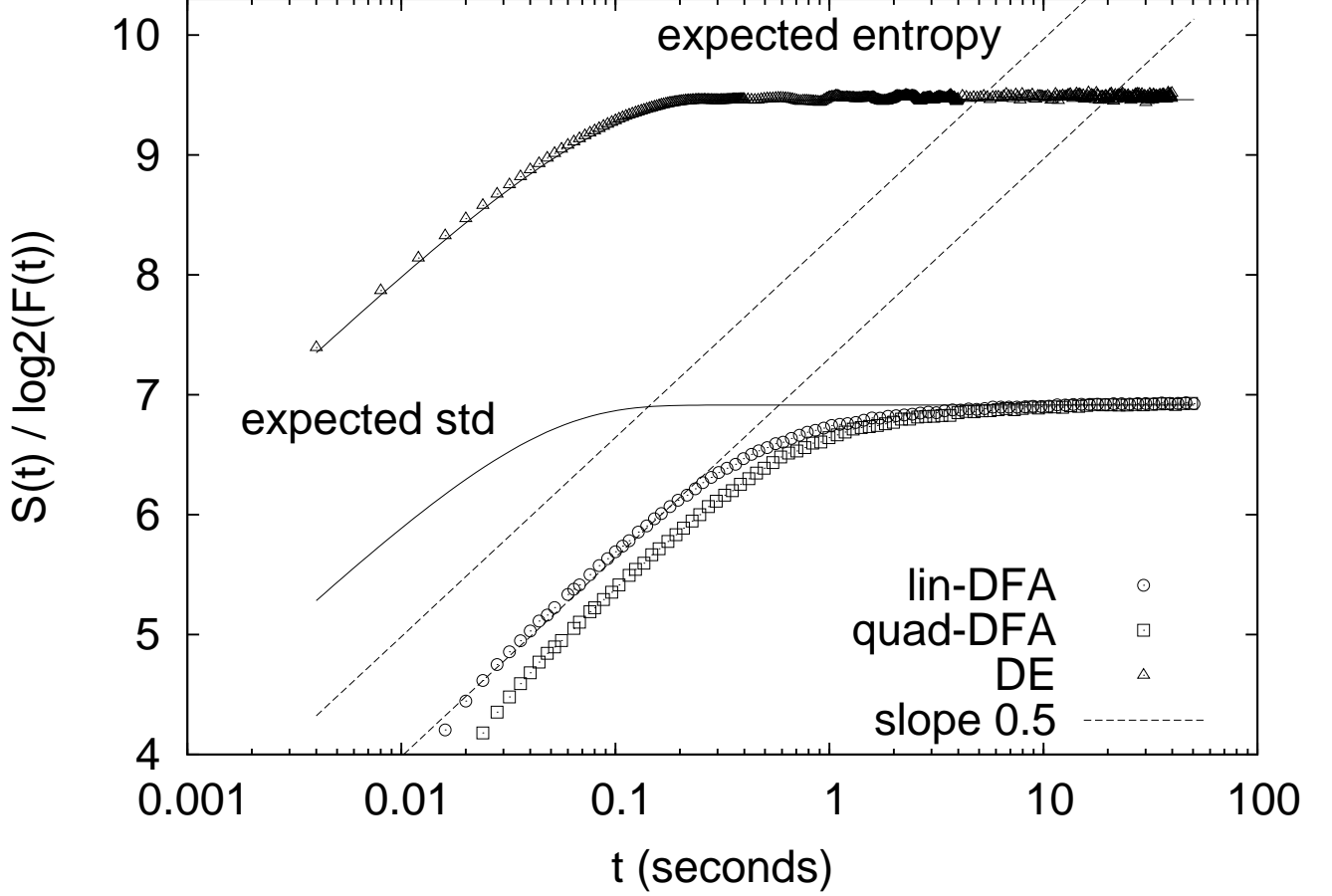


FIG. 6: DE and DFA for the increments of the variable $X(t)$ of Eq. (1) with $\lambda=0.055$ and $D=800$. The triangles indicates the values of the entropy $S(t)$, while circles (linear detrending) and squares (quadratic detrending) are the values of base-2 logarithm of the variance $F(t)$. The solid lines are the expected values for $S(t)$ and $\log_2(F(t))$. The dashed line indicates a logarithmic increase with a slope 0.5.

Most studies in the literature, however, report results of the application of DFA to the EEG time series itself. Thus, we too apply DE and DFA to the variable $X(t)$ of Eqs. (1) and (16), and to the EEG itself as well.

Fig. 8 show the application of DE and DFA to the variable $X(t)$ satisfying Eq. (1). The solid lines represent the expected values for the standard deviation. These are obtained by integrating the variable $X(t)$

$$Y(t) = \int_0^t X(t') dt' = \int_0^t dt' e^{-\lambda t'} \int_0^{t'} \eta(t'') e^{\lambda t''} dt'' \quad (25)$$

and calculating the variance $\sigma_Y^2(t)$:

$$\sigma_Y^2(t) = \frac{D}{\lambda^3} [2\lambda t + 4e^{-\lambda t} - e^{-2\lambda t} - 3]. \quad (26)$$

Using Eq. (26), we obtain for times $t \ll 1/\lambda$

$$\lim_{t \rightarrow 0} \sigma_Y^2(t) = \frac{2}{3} D t^3, \quad (27)$$

while for $t \gg 1/\lambda$

$$\lim_{t \rightarrow \infty} \sigma_Y^2(t) = \frac{2D}{\lambda^2} t - \frac{3D}{\lambda^3}. \quad (28)$$

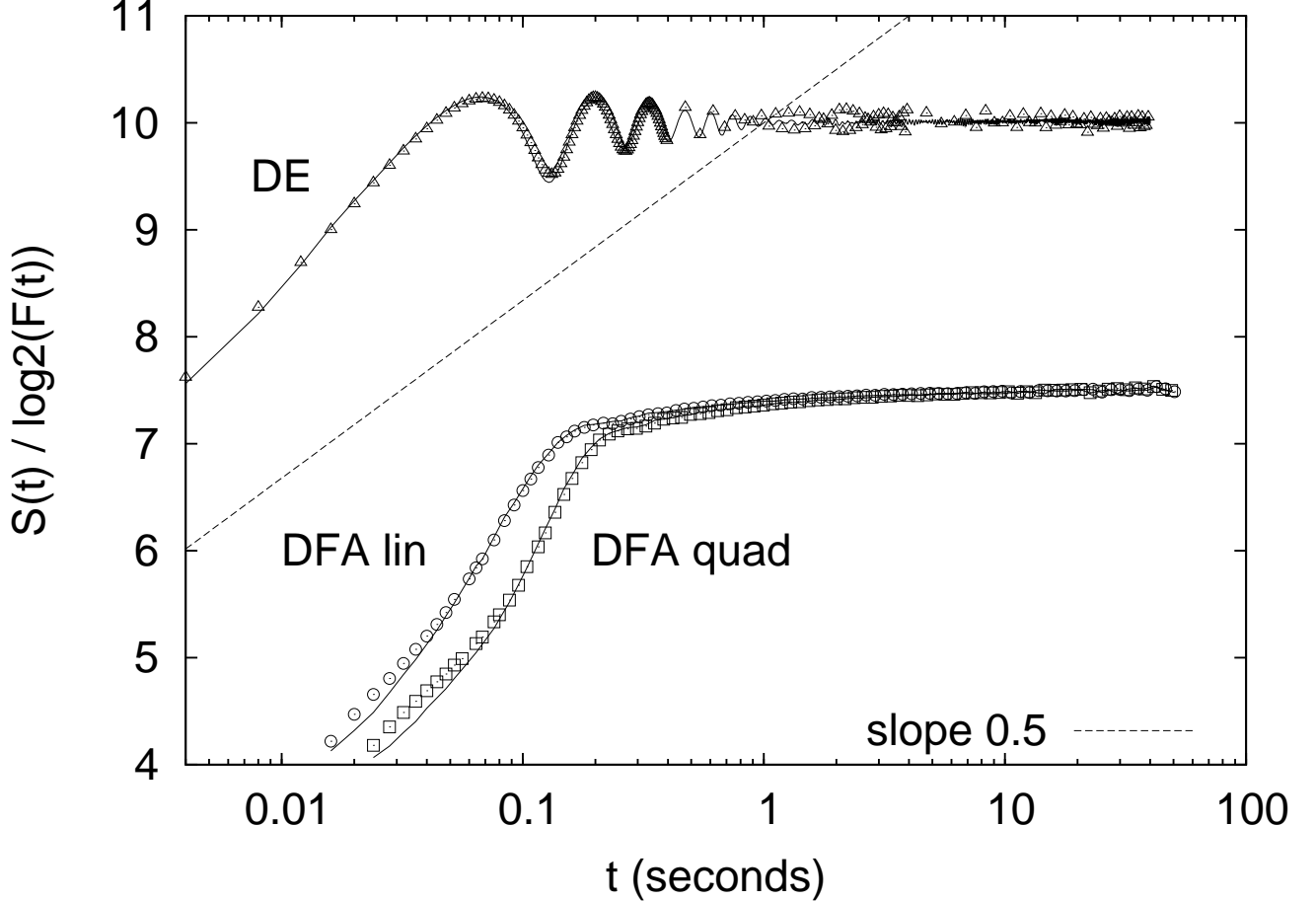


FIG. 7: DE method and DFA for the increments of a EEG record (channel O1) and the increments of its best approximation via the model of Eq. (16) (Section II C). Solid lines indicate the results of DE and DFA relative to the EEG record. Triangles indicate the results of DE calculation relative to the Ornstein-Uhlenbeck process of Eq. (16) approximating the EEG record, while circles (linear detrending) and squares (quadratic detrending) indicate those of DFA. Finally, the dashed line indicates a logarithmic increase with a slope of 0.5.

Finally, since $Y(t)$ is a Gaussian variable for all time t we can obtain the value of the diffusion entropy $S(t)$ using Eq. (9). We see from Fig. 7 that the numerical diffusion entropy (triangles) departs from the theoretical expectations at early times ($t \ll 1/\lambda$). In fact the initial slope of the numerical diffusion entropy is ~ 1 (0.96 for $t < 0.04s$) instead of 1.5 as expected from Eq. (27). This is due to the overlapping window procedure used by DE [31]. For times $t \gg 1/\lambda$ the numerical diffusion entropy reproduces the expected results (slope 0.51 for $0.4s < t < 1s$): the discrepancy for times $t > 3s$ is due to the finiteness of the record used.

The DFA curves seems to reproduce both the early time scaling and the later time scaling: the initial slope is 1.4 ($0.01s < t < 0.1s$), while for $2s < t < 10s$ the DFA curves have slope 0.52. The major discrepancy between the numerical DFA curves and the expected behavior for $\log_2 F(t)$ (aside from the shift in values) is that the scaling regime with parameter ~ 0.5 is delayed one decade in time ($\sim 2s$ instead of $\sim 0.4s$). This effect also occurred for in the case of the increments of the variable $X(t)$ of Eq. (1) (Fig. 4). Fig. 9 shows the results of the DE method and DFA for a EEG record (channel O1) and its best approximation via the model of Eq. (16) (Section II C). Since the DE algorithm does not have any detrending procedure the presence of an alpha rhythm produces modulation observed for $t \lesssim 1s$ both for the real EEG (solid line) and the its approximation (squares). The DE of the EEG and that of the model depart at $\sim 0.8 - 1s$: the EEG entropy saturates while the model DE continues to increase. The DFA of the real EEG shows a double “scaling” regime for the DFA ($t \lesssim 0.1s$ and $0.4s \lesssim t \lesssim 4s$). At $t \sim 4s$ a split, similar to that observed in the DE at $t \sim 1s$, occurs between the DFA of the EEG which saturates and that of the model which continues to increase. The slope (we report the values for the DFA with linear detrending as the values for the quadratic detrending are similar) of the first scaling regime is 1.75 for the EEG record and 1.73 for the model approximation. The second scaling regime

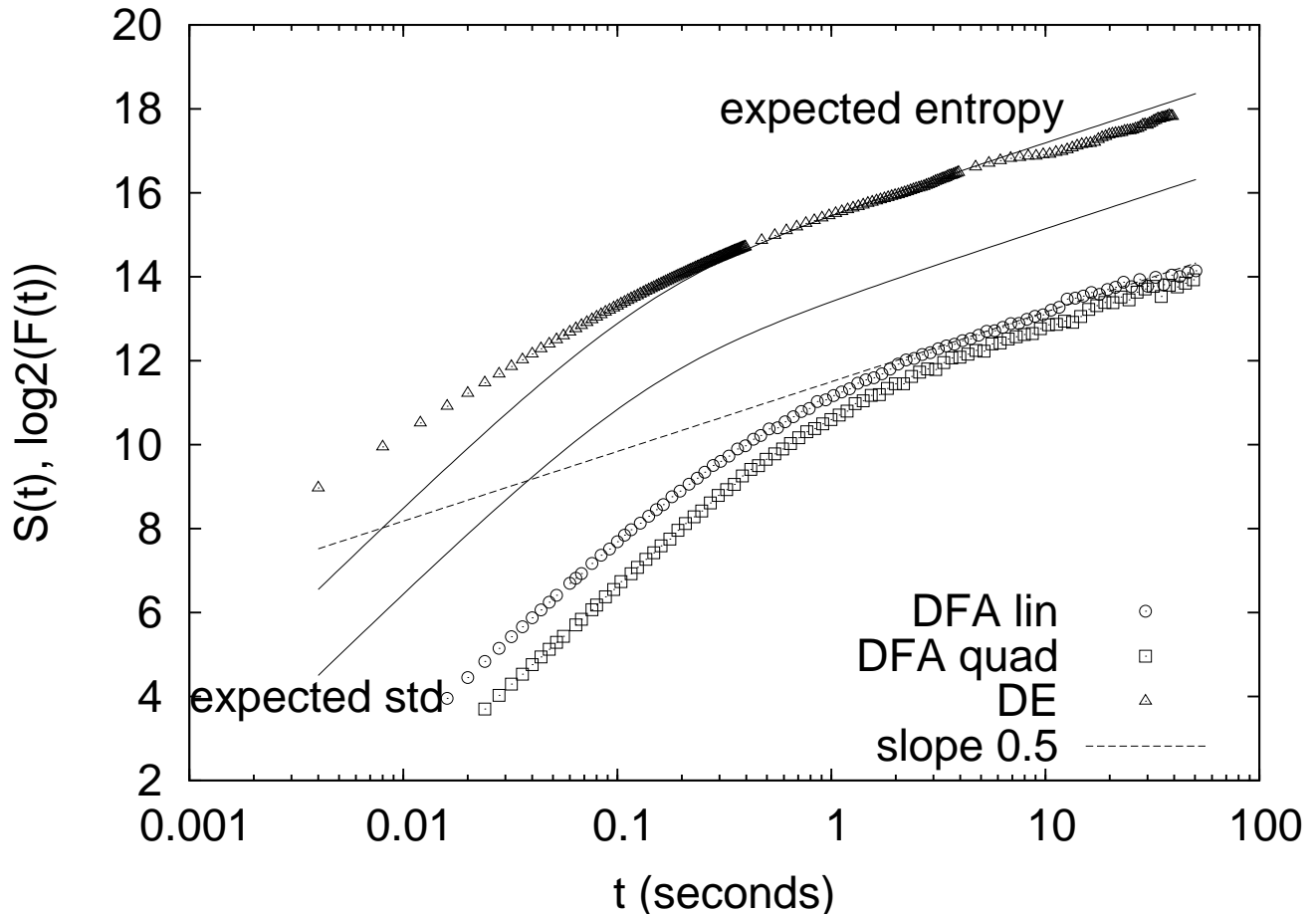


FIG. 8: DE and DFA for the variable $X(t)$ of Eq. (1) with $\lambda=0.055$ and $D=800$. The triangles indicates the values of the entropy $S(t)$, while circles (linear detrending) and squares (quadratic detrending) are the values of base-2 logarithm of the variance $F(t)$. The solid lines are the expected values for $S(t)$ and $\log_2(F(t))$. The dashed line indicates a logarithmic increase with a slope 0.5.

has a slope of 0.65 for the EEG and 0.64 for the model approximation. Are these genuine scaling regimes? As in the similar case presented in Fig. 9, these linear regime are not genuine scaling regimes but are the result of the EEG dynamics not satisfying the decomposition of Eq. (17) which compromises the capability of the DFA to detrend the alpha-wave component. For times $t > 4s$ the DFA curve relative to the EEG starts to bend so that a linear fit is not feasible. However the model approximation curves keep increasing. The nature of the saturation observed for both DE and DFA in Fig. 9 has been recently explained [32] as being due to high-pass filtering by the EEG recording apparatus. Valencia *et al.* [32] show that the saturation time for the DFA of the EEG record is simply the inverse of the cutoff frequency f_c of the high-pass filter: 0.3Hz in the present case.

IV. COHERENCE OF ALPHA WAVE

Nikulin and Brismar [16] use the Hilbert transform of EEG time series to define a sequence of EEG amplitudes, which is then filtered to obtain a sequence of alpha rhythm amplitudes. DFA is then applied to this latter sequence to find scaling in the 5 – 50s range. The scaling parameters change within each channel of a single subject and among subjects: 0.71 median with a quartile range 0.63 – 0.81. Linkenkaer-Hansen et al. [15] apply the DFA to the sequence of the moduli of the wavelet transform of the EEG signal in the scale range corresponding to the alpha rhythm (8.3 – 11.7Hz). They report a scaling parameter of 0.68 ± 0.07 (average over the subjects and channels) in the 5 – 300s time range. In Fig. 10 we report the autocorrelation function for the times series of the amplitudes A_j and frequency f_j for the alpha rhythm for two different channels: O1 and C3. Each couple $\{A_j, f_j\}$ represents the

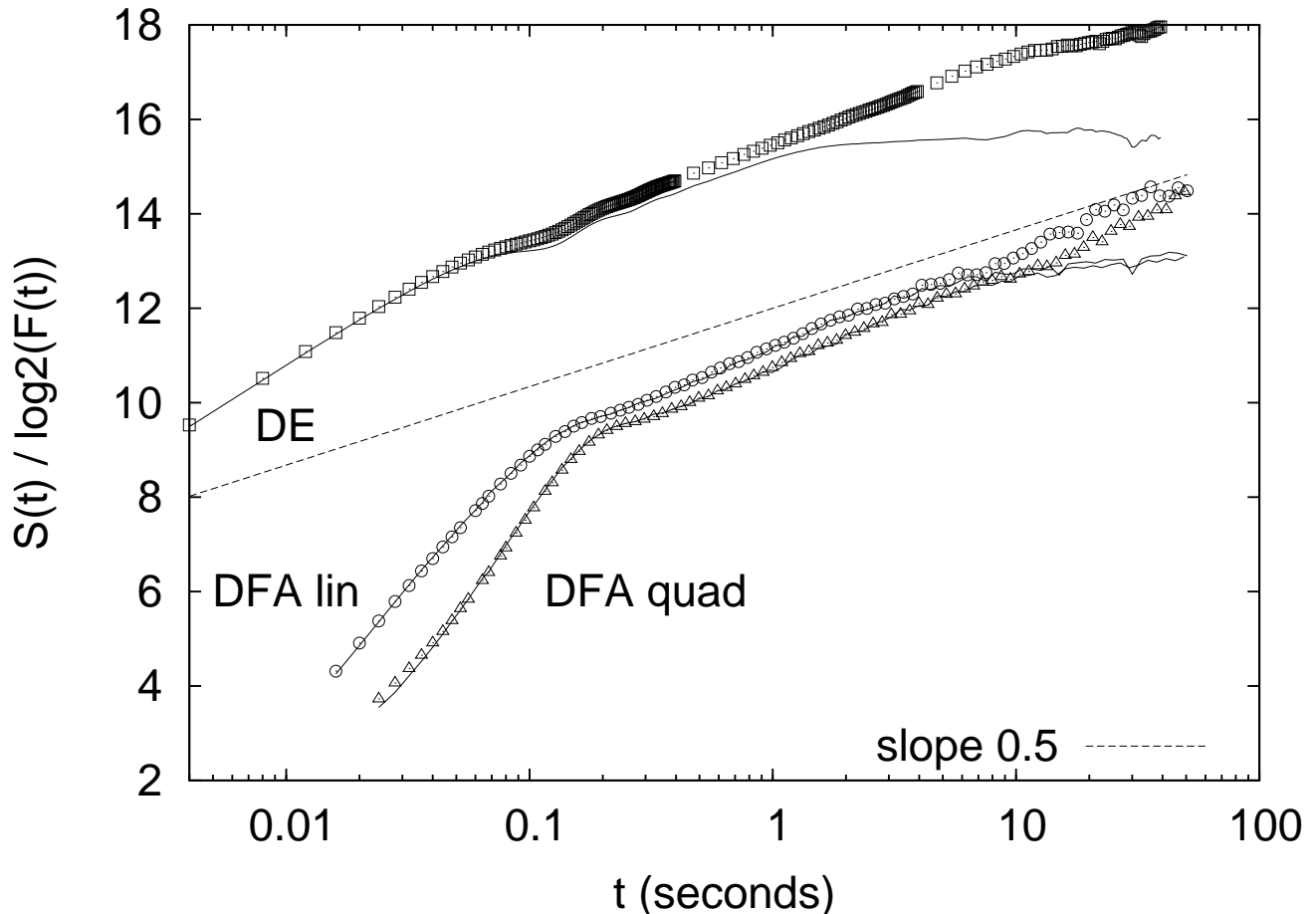


FIG. 9: DE method and DFA for a EEG record (channel O1) and its best approximation via the model of Eq. (16) (Section II C). Solid lines indicate the results of DE and DFA relative to the EEG record. Triangles indicate the results of DE calculation relative to the Ornstein-Uhlenbeck process of Eq. (16) approximating the EEG record, while circles (linear detrending) and squares (quadratic detrending) indicate those of DFA. Finally, the dashed line indicates a logarithmic increase with a slope of 0.5.

amplitude and frequency of the alpha rhythm during 0.5s of EEG activity (see Section II C). Fig. 10 shows fast decay for the autocorrelation of both the amplitudes and the frequencies of each channel. The autocorrelation drops to $\sim 0.1 - 0.2$ at a lag of ~ 10 (which correspond to a coherence time of ~ 10 s) after which the autocorrelation function oscillates in the range $(-0.2, 0.2)$. To quantify the strength of the correlation between the sequences A_j and f_j we shuffle the two time series and use Eq. (16) to create a surrogate record. In Fig. 11 we compare the DE for the EEG increments (channel O1), with its best approximation via Eq. (16) and the surrogate data obtained applying Eq. (16) to a shuffled sequence of couples $\{A_j, f_j\}$. We see how shuffling the couples $\{A_j, f_j\}$ results in a sharper attenuation of the periodic alpha modulation, but does not change the qualitative results.

V. DISCUSSION AND CONCLUSIONS

The first notable property of the OU Langevin model of EEG time series is that the resulting EEG diffusive entropy reaches a saturation level. The EEG entropy saturation indicates that the EEG time series asymptotically carries a maximum amount of information. Robinson [14] observed this saturation in the calculation of second moments of EEG time series and interpreted it as being due to dendritic filtering. The EEG entropy does not grow indefinitely as would a random process with long-time correlation; consequently, the EEG time series do not simply scale as had been previously assumed by a number of investigators [4, 5, 8].

Schlögl et al. [18] remarked that biosignals typically saturate due to the limited dynamic range of amplifiers and

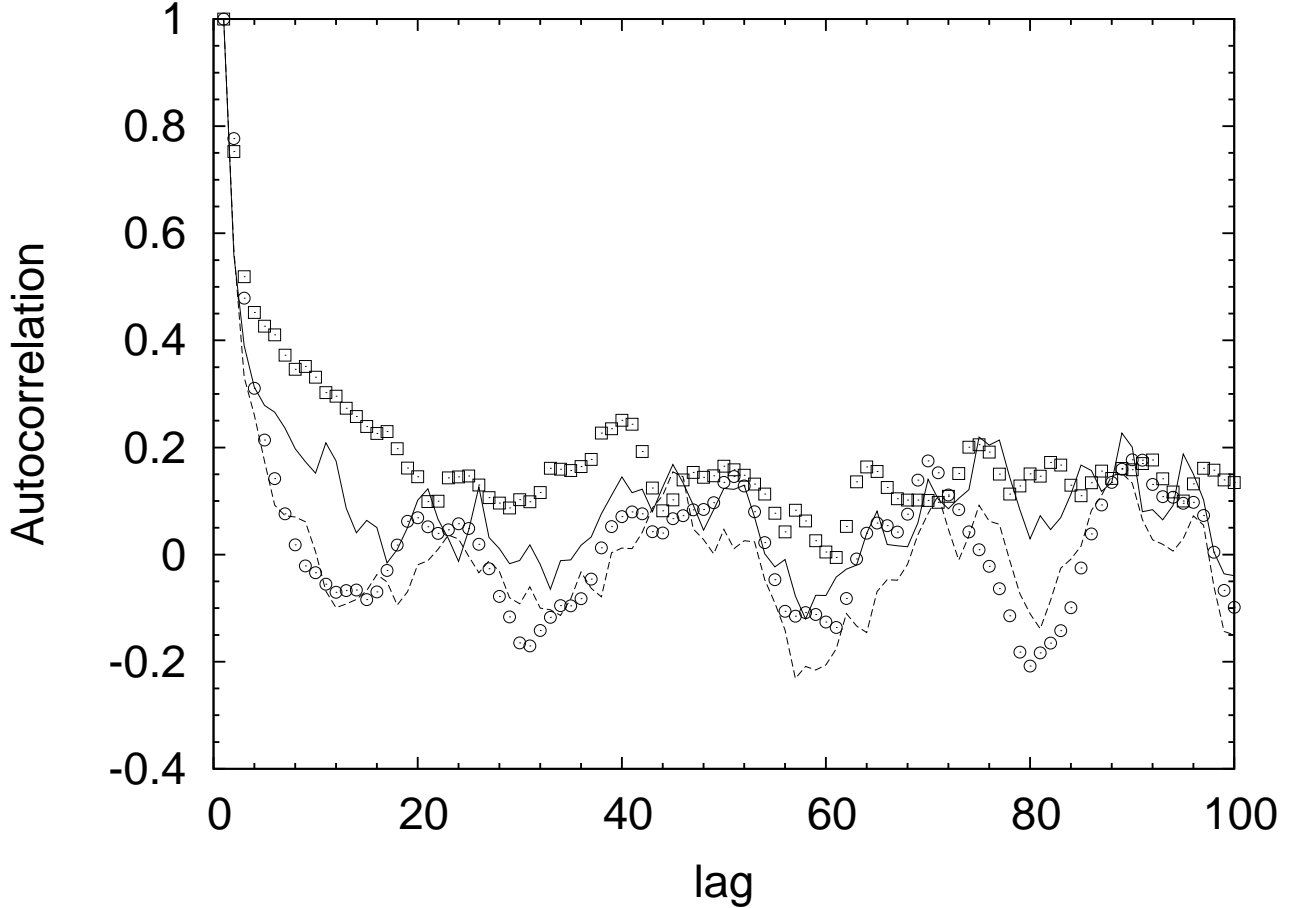


FIG. 10: Autocorrelation function for the sequence of amplitudes and frequencies of the alpha rhythm for the channels O1 and C4: empty squares (circles) indicate the autocorrelation function of the sequence A_j , and solid (dashed) lines the autocorrelation function of the sequence f_j for the channel O1 (C4).

observed the saturation of EEG entropy during sleep using data from eight European laboratories. However we find that the time constant for saturation due to the limited dynamic range of the amplifier is significantly larger than that due to physiologic processes in the brain as indicated by the lack of saturation in Fig. 8. How does this filtering procedure affects the observed results for the DE and DFA of the EEG increments (Fig. 6)? Is the saturation effect observed for the DE of the EEG increments genuine or is it an artefact of high pass filtering? Table I reports the typical values observed for the dissipation parameter λ of the Eq. (16) used to fit the observed DE curve relative to EEG increments. The time $1/\lambda$ is the “saturation” time of the DE curve as shown by Eq. (5). The time $1/\lambda$ can be considered as the “saturation” time even when an alpha-wave component is present in the EEG record, since this results in a periodic modulation to Eq. (5). Recalling that our EEG records are sampled at 250 Hz, and that from table I the value $0.04Hz$ can be considered as a typical value for the parameter λ , we obtain a typical saturation time of the order of $0.1s$ which is considerably smaller than the saturation time $1/(0.3Hz) \simeq 3.3s$ due to the high-pass filtering.

The second notable property of the OU Langevin model is related to the first and is the dissipation, or negative feedback, produced locally within the channel of interest. The fluctuation-dissipation relation of Einstein quantifies the maximum level of the entropy in a closed physical network, and is given by the ratio of the strength of the additive fluctuations to the dissipation rate. In the more general OU driven Langevin equation given here we do not expect the saturation level to be given by this ratio alone, but to depend on the asymptotic value of the ‘variance’ $\sigma(t \rightarrow \infty)$. Note that the asymptotic ‘variance’ may not be independent of time, but contains residual information in the form of low amplitude beats because of its dependence on the random near-periodic driver. This mechanism also explains the saturation observed earlier [14] by associating the negative feedback with the dendritic filtering of the signal.

The third notable feature of the OU Langevin model is the attenuated oscillation of the entropy in time. We

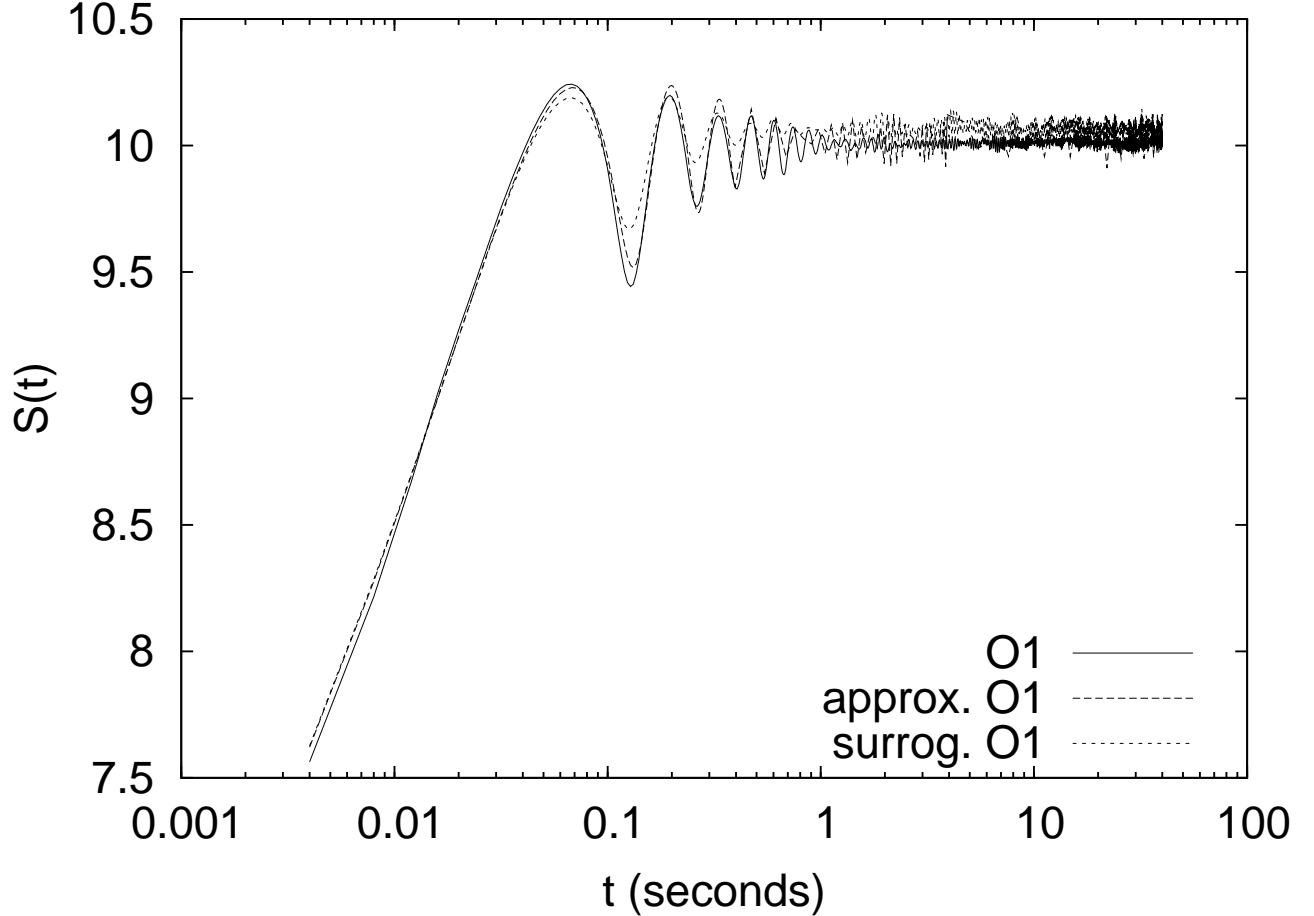


FIG. 11: Comparison of DE applied to the increments time series: solid line (EEG channel O1), dashed line (best approximation via Eq. (16) and, dot-dashed line (surrogated data obtained applying Eq. (16) to a shuffled sequence of couples $\{A_j, f_j\}$).

reasonably interpret the attenuation of the modulation of the EEG entropy to be a consequence of the alpha rhythm not being generated at a single source, but to be a collective property of the brain being generated at a number of different locations [10, 19]. Here the influence of the distributed sources is modeled by wave packets that persist for a stability time t_s ; one packet is replaced by another with a slightly different carrier frequency and amplitude chosen from the empirical spectrogram over time intervals of length t_s . The concatenation of these wave packets with fluctuating frequencies and amplitudes produces a decoherence that attenuates the modulation of the resulting EEG entropy in time. Both Figures 10 and 11 indicate that the attenuation of the alpha rhythm is dependent on the statistics of the amplitude and frequency fluctuations and not on their statistics.

The presence of alpha-rhythm modulation masks [24] any early-time scaling property of the EEG dynamics. Eq. (16) is the simplest form of a fluctuation-dissipation process that implies the presence of internal feedback to prevent the occurrence of large excursions of the electric potential inside the brain. The presence of this negative feedback mechanism casts doubt on the possibility of understanding EEG records in terms of a sum of two independent components, noise and trend (signal), which is the usual assumption made for the DFA method.

Finally, the analysis presented herein supports the notion that alpha rhythms [10] are not passive states, but contain useful information within the frequency modulation.

The authors thank the Army Research Office for support of this research. The code of the programs used for the EEG

analysis (DE and spectrogram) is available at http://www.duke.edu/~mi8/softwaresubpage/C++_programs.html

-
- [1] N. Wiener, *Nonlinear Problems in Random Theory*, MIT Press and John Wiley, New York (1958).
 - [2] B.J. West, *Fractal Physiology and Chaos in Medicine*, World Scientific, Singapore (1990).
 - [3] W.J. Freeman, *Mass Action in the Nervous System*, Chapter 7, Academic Press, New York pp 489 (1975).
 - [4] R. C. Hwa and T. H. Ferree, *Phys. Rev. E*, **66**, 021901 (2002).
 - [5] J. M. Lee, D. J. Kim, I. Y. Kim, K. S. Park and S. I. Kim, *Computers in Biol. and Medicine*, **32**, 37 (2002).
 - [6] P. A. Watters and F. Matin, *Biol. Psych.* **66**, 79 (2004).
 - [7] M. Stead, G. A. Worrel and B. Litt, *Complexity* **10**, 35 (2005);
 - [8] J. W. Yuan, B. Zheng, C.P. Pan, Y. Z. Wu and S. Trimper, *Phys. A*, **364**, 315 (2006).
 - [9] E. Başar, *Int. J. Psychophys.* **60**, 133 (2006).
 - [10] E. Başar, M. Schürmann, C. Başar-Erouglu and S. Karakaş, *Int. J. Psychophys.* **26**, 5 (1997).
 - [11] C. K. Peng, S.V. Buldyrev, S. Havlin, M. Simons, H. E. Stanley and A. L. Golberger, *Phys. Rev. E*, **49**, 1685 (1994).
 - [12] M. Buiatti, D. Papo, P.-M. Baudonniere and C. van Vreeswijk, *Neuroscience*, **146**, 1400 (2007).
 - [13] S. Cai, Z. Jiang, R. Zhou, P. Shou, H. Yang and B. Wang, *Phys. Rev. E*, **76**, 061903 (2007).
 - [14] P. A. Robinson, *Phys. Rev. E* **67**, 032902 (2003).
 - [15] K. Linkenkaer-Hansen, V. V. Nikouline, J. M. Palva and R. J. Ilmoniemi, *J. Neuroscience*. **21**, 1370 (2001).
 - [16] V.V. Nikulin and Brismar T, *Neuroscience*. **130**, 549 (2005).
 - [17] T. Inouye, K. Shinosaki, H. Sakamoto, S. Toi, S. Ukai, A. Iyama, Y. Katzuda, and M. Hirano, *Electroenceph Clin. Neurophys.*, **79**, 204 (1991).
 - [18] A. Schlögl, B. Kemp, T. Penzel, S. Kunz, S. Himanen, A. Värri, G. Dorffner and G. Pfurtscheller, *Clinical Neurophys.* **110**, 2165 (1999).
 - [19] P. Patel, D. Khosla, L. Al-Dayeh and M. Singh, *Clinical Neurophys.* **110**, 538 (1999).
 - [20] O.A. Rosso, S. Blanco, J. Yordanova, V. Kolev, A. Figliola, M. Schürmann and E. Başar, *J. Neurosci. Meth.* **105**, 65 (2001).
 - [21] O.A. Rosso, *Int. J. Psychophys.* **64**, 75 (2007).
 - [22] M. Ignaccolo, M. Latka, W. Jernajczyk, P. Grigolini and B.J. West,
 - [23] N. Scafetta, P. Hamilton, P. Grigolini, *Fractals* **9**, 193 (2001); P. Grigolini, L. Palatella, G. Raffaelli, *Fractals* **9**, 439 (2001).
 - [24] M. Ignaccolo, P. Allegrini, P. Grigolini, P. Hamilton, and B. J. West, *Physica A*, **336**, 595 (2004); M. Ignaccolo, P. Allegrini, P. Grigolini, P. Hamilton, and B. J. West, *Physica A*, **336**, 623 (2004).
 - [25] P. Grigolini, D. Leddon and N. Scafetta, *Phys. Rev. E* **65**, 046203 (2002).
 - [26] N. Scafetta and B. J. West, *Phys. Rev. Lett.* **90**, 248701 (2003).
 - [27] K. Lindenberg and B.J. West, *The Nonequilibrium Statistical Physics of Open and Closed Systems*, VH, New York (1990).
 - [28] C.E. Shannon, *Bell Sys. Tech. J.* **27**, 379-423; *ibid* 623-656 (1948).
 - [29] N. Wiener, *Cybernetics*, MIT Press, Cambridge, MA (1948).
 - [30] S. Mallat, *A wavelet tour of signal processing* 2nd Editon, Academic Press, San Diego (1999)
 - [31] The discrepancy between the observed behavior of the DEA and the theoretical one is due to the overlapping window algorithm, Eq. (12) used in the DEA.
 - [32] M. Valencia, J. Artieda, M. Alegre and D. Maza, *J. Neurosc. Methods*, **170**, 310 (2008).